ACS OMEGA

http://pubs.acs.org/journal/acsodf

Article

Fabrication of Densified Rice Husk by Sequential Hot-Compressed Water Treatment, Blending with Poly(vinyl alcohol), and Hot Pressing

Qianli Wang, Shinji Kudo, Shusaku Asano, and Jun-ichiro Hayashi*

Cite This: *ACS Omega* 2022, 7, 27638–27648

Read Online

ACCESS | Metrics & More | Article Recommendations | Supporting Information

ABSTRACT: Processing agricultural wastes into densified materials to partially substitute wooden product production is significant for reducing the consumption of forest resources. This work proposes the fabrication of high-strength rice husk (RH)-based composite materials with poly(vinyl alcohol) (PVA) via densification by hot pressing. RH was pretreated in hot-compressed water (HCW) prior to pulverization and blending with PVA or PVA/glycerol (GL). The incorporation of PVA greatly improved the strength, toughness, and waterproofness of the composite plate, which was discussed with the help of a variety of composite characterizations. The tensile strength, flexural strength, and toughness of a composite of HCW-treated RH, PVA, and GL with a mass ratio of 80:20:2 were 42, 81 MPa, and 5.9 MJ/m^3, respectively. The HCW treatment and blending with PVA and GL improved those properties of the hot-pressed original RH plate by factors of 2.5, 2.3, and 6.7, respectively, and reduced the water uptake and swelling ratio in water by 57 and 53%, respectively, despite the hydrophilic nature of PVA and GL. Altogether, this work outlines a valuable and sustainable approach to the efficient utilization of agricultural wastes.

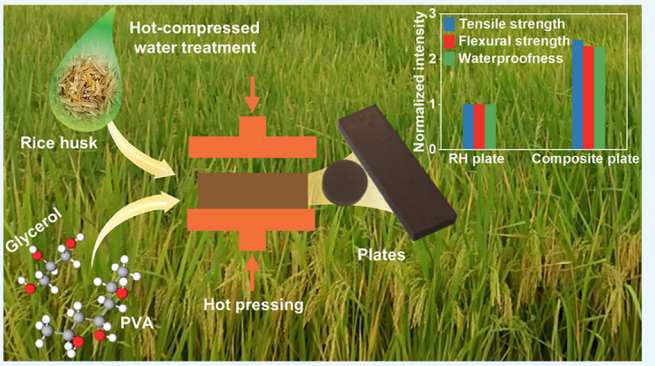

1. INTRODUCTION

Biomass-based materials have received much attention due to their sustainability against a background of increasingly serious environmental issues. Common agricultural waste, lignocellulosic biomass, is often regrettably incinerated or landfilled, resulting in not only underuse of this resource but also environmental problems.[1,2] Recently, the fabrication of boards based on nonwoody biomass has attracted increased interest, such as rice straw,[3] wheat straw,[4,5] corn stalk,[6] bamboo,[7] and hemp shiv boards.[8] These materials can partially replace wood-based boards. Rice husk (RH), which is a byproduct of rice milling, has received specific attention owing to its abundance, around 120 million tons of which is produced annually.[9] However, in view of the poor mutual adhesion of RH, the strength and water resistance of densified RH materials are not satisfactory, hindering its practical applications.[10,11]

Current industries often employ formaldehyde-based resin as a binder to improve the mechanical performance of lignocellulosic boards, but this has been criticized because such materials easily release toxic formaldehyde, posing a risk to human health.[12] Consequently, different strategies have been explored to fabricate composites with less or minimal environmental impact.[13] For instance, some biodegradable binders are often incorporated into biomass composite to improve strength, such as soybean protein,[14] starch,[15] and polylactic acid.[16] Although such binders promote the strength of the composites, maintaining their biodegradable property, it is necessary to improve their resistance to water and humidity. In addition, functional biomass-based composites with general-purpose polymers, including recycled high-density polyethylene (HDPE),[17,18] polypropylene (PP),[19,20] and poly(vinyl chloride) (PVC),[21] not only have relatively high strength but also contribute to the recycling of plastics. However, such composites also encounter poor compatibility between the biomass and polymer matrix as well as extremely difficult biodegradation. Additional modification of biomass, or polymer resin, is, therefore, necessary to improve the affinity between these materials. Some mechanical and chemical pretreatments of biomass were studied previously.[22,23] The present authors investigated hot-compressed water (HCW) treatment of RH and demonstrated its effectiveness in enhancing the mechanical strength of densified RH fabricated by pulverization and hot pressing in sequence. The HCW

Received: May 26, 2022
Accepted: July 20, 2022
Published: July 28, 2022

https://doi.org/10.1021/acsomega.2c03286
ACS Omega 2022, 7, 27638–27648

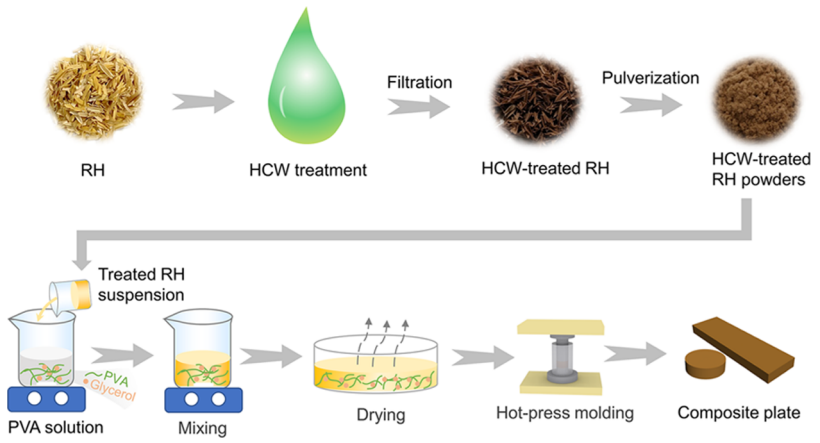

Figure 1. Schematic illustration of experimental processes for preparing the densified RH composite plate.

greatly improved the pulverizability of RH, inducing the appearance of a fibrous self-reinforcement material and optimizing the ratio of the reinforcement material (≈cellulose and silica) to the matrix (≈lignin + hemicellulose).[24] Based on previous investigations, it was believed that an appropriate type of biodegradable polymer could act as a binder in enhancing the above-mentioned mechanical properties of the densified RH.

Poly(vinyl alcohol) (PVA) is a relatively cheap, biodegradable thermoplastic polymer with high chemical resistance, showing great potential in industrial applications.[25,26] PVA is also a water-soluble polymer rich in hydroxyl groups, which can offer strong physical cross-links via hydrogen bonds with oxygen-containing functional groups of cellulose, lignin, and even silica in the resulting composite, enhancing its mechanical strength.[27] PVA has a Hildebrand solubility parameter much closer to cellulose and lignin than other general-purpose plastics, which is conducive to the miscibility of PVA and biomass matrix in processing.[28,29] For example, rubberwood particleboard bonded with a mixture of modified starch and PVA has greater mechanical strength and higher dimensional stability than that with starch alone.[30] Wu et al. prepared a composite through hydrogen-bond cross-linking between lotus fibers and PVA. The cross-links improved the mechanical strength.[31] In addition, Zhang et al. reported increases in the tensile strength, toughness, and thermal stability of a type of PVA film by adding lignin nanoparticles, which were dispersed in the PVA matrix being hydrogen-bonded to the matrix.[32] However, to the best of our knowledge, PVA has been barely used as a binder in agricultural waste to fabricate green densified materials.

In this work, PVA was incorporated into HCW-treated and pulverized RH to fabricate densified plates through hot-press molding, as schematically illustrated in Figure 1. The pretreatment of RH, if it improves compatibility with PVA, is significant. It was expected that the HCW treatment loosened the association among cellulose, hemicellulose, lignin, and silica of RH, inducing more frequent bonding to PVA as well as enhancing moldability.[22,33] The HCW-treated RH and PVA were mixed homogeneously by a wet method with water and dried and molded into plates by hot pressing. The addition of a small amount of glycerol (GL) facilitated the incorporation of PVA into the RH matrix.[34] The effects of PVA addition on the mechanical properties and waterproofness of the plate were examined and discussed.

2. EXPERIMENTAL SECTION

2.1. Materials. RH was supplied from a farm in Ishinomaki, Miyagi Prefecture, Japan. It was pulverized into sizes of 0.85−2 mm and used as the feedstock. PVA (Mowiol 20−98, M_w ∼125,000) was sourced from Sigma-Aldrich. Sodium hydroxide, glycerol, and 95% sulfuric acid were from Fujifilm Wako Pure Chemical Corporation and used without further purification.

2.2. HCW Treatment of RH. The HCW treatment of RH was described in detail in our previous paper.[24] Briefly, 25 g of RH was charged into a percolator and was extracted with HCW at 160 °C and 5 MPa for 2 h, flowing at a rate of 30 mL/min. After quenching, the collected solid was washed with deionized water (electroconductivity; 18.2 MΩ) and dried in air and then under vacuum at 50 °C for 24 h. The HCW-treated RH prepared in this way is referred to as RHW. As a reference, RH was also subjected to a batch-wise treatment in an aqueous solution of 1 M NaOH at a solid/liquid ratio of 1/20 at 25 °C for 2 h. The treated solids were washed with deionized water and dried in the same way as above. This alkali-treated RH is termed RHA.

2.3. Preparation of RH-Based Composites. RH, RHW, and RHA were ground to sizes smaller than 38 μm (equivalent to 400 mesh). The prescribed amount of PVA or PVA/GL mixture (mass ratio; 10/1) was dissolved in 40 mL of deionized water at 93 °C. The obtained solution was suspended with RH, RHW, or RHA at a solid/liquid ratio of 1/10, and the suspension was stirred for 2 h at 30 °C. It was then spread on a glass-made dish, dried at 50 °C, and ground into powders. The compositions of RH and composites are summarized in Table 1.

2.4. Hot-Press Molding. The powder of each material shown in Table 1, which contained 10−15 wt % moisture, was loaded into a cylindrical or rectangular mold and hot-pressed

Table 1. Mass Fractions of RH, RHW, PVA, and GL in Blending

sample	ground RH (wt %)	PVA (wt %)	GL (wt %)
RH	100		
RH/PVA20	80	20	
RHA/PVA20	80	20	
RHW/PVA20	80	20	
RHW/PVA20/GL2	80	20	2

https://doi.org/10.1021/acsomega.2c03286
ACS Omega 2022, 7, 27638−27648

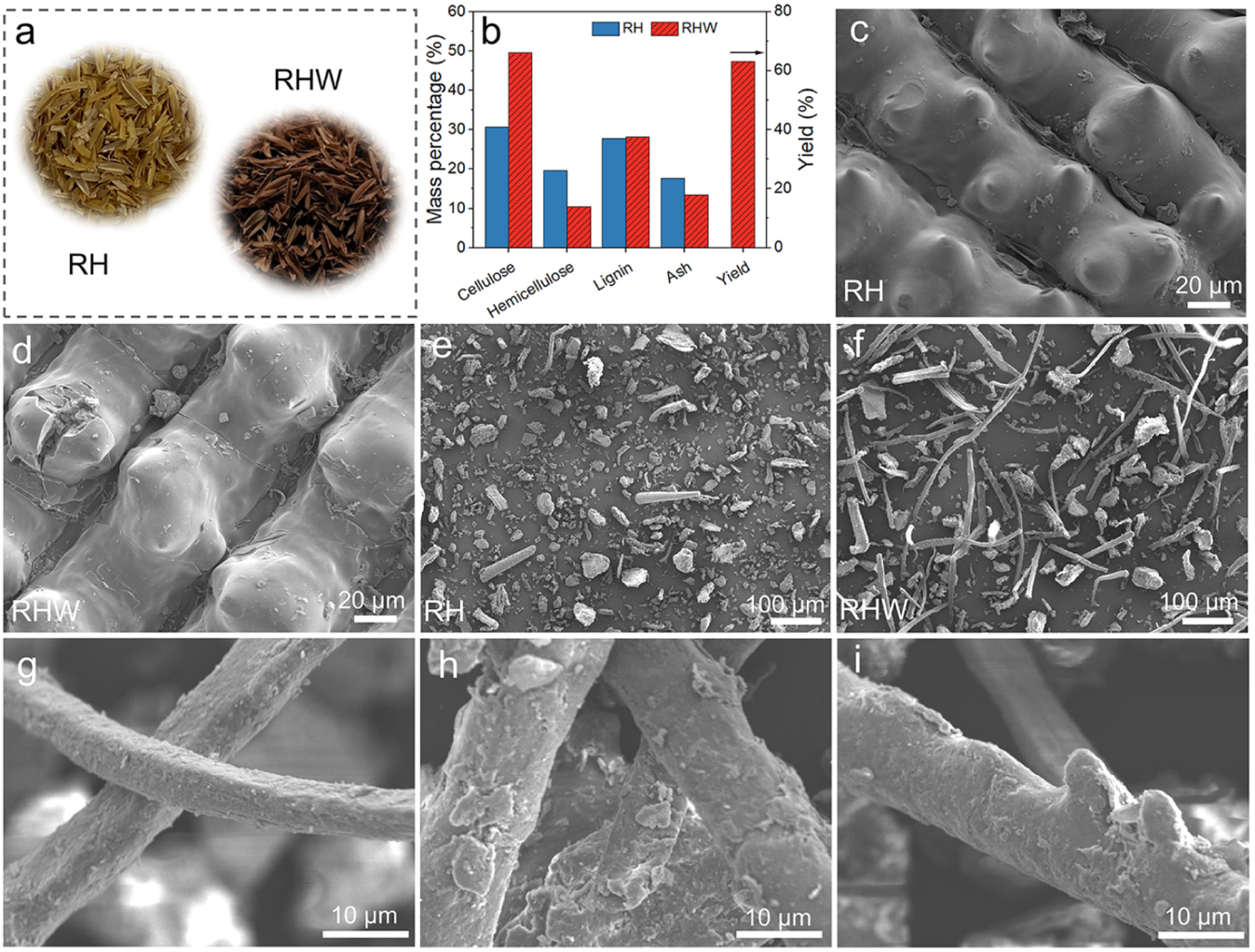

Figure 2. Appearances of RH and RHW (a), chemical compositions of RH and RHW (b), and SEM micrographs of RH and RHW before (c, d) and after (e, f) pulverization. SEM photographs of fibers of RHW (g) after blending with PVA (h) and with PVA/GL (i).

to prepare a circular plate (dimension; Φ 14 mm × ca. 4.4 mm height) or a rectangular one (35 mm long × 10 mm width × ca. 3.5 mm thickness), respectively. The temperature, mechanical pressure, and time for the hot-press molding were 200 °C, 250 MPa (cylindrical mold) or 112 MPa (rectangular mold), and 8 min, respectively. After cooling, the plates were demolded and stored at an ambient temperature and in air with a relative humidity of 50% until the moisture content became steady at an equilibrium moisture content.

2.5. Characterization. *2.5.1. Physicochemical Property Measurement.* Materials before or after hot pressing were characterized as mentioned below. Fourier transform infrared spectroscopy (FTIR) spectra were acquired on a PerkinElmer Spectrum-Two spectrometer with an attenuated total reflectance accessory available over a wavenumber range of 500−4000 cm^{-1}. The specimens were dried prior to measurement. Powder X-ray diffraction (XRD) patterns were taken within a range of 5−50° on a Rigaku TTR-III applying Cu Kα radiation. Thermogravimetric analysis (TGA) was carried out on a Hitachi Hi-Tech Science model (STA7200) with a heating rate of 5 °C/min and a peak temperature of 700 °C in the flow of atmospheric air or nitrogen (purity > 99.9999 vol %, flow rate = 300 mL/min). Differential scanning calorimetry (DSC) was performed on a Netzsch 204 F1 model with a heating rate of 10 °C/min over a temperature range of 30−250 °C. The chemical compositions of RH and RHW were determined by a two-stage hydrolysis that was recommended by the National Renewable Energy Laboratory (NREL).[35] The ash content was determined by a general combustion method that involved mild but complete combustion in air at 575 °C for 3 h.

Hot-pressed materials were also characterized by simple combustion tests to evaluate fire resistance. A side of the rectangular plate was exposed to flame from an alcohol lamp for 30 s. The behavior of each specimen was video-recorded (see the Supporting Information).

Fracture surfaces of hot-pressed materials (after strength measurements) were observed by scanning electron microscopy (SEM) on a JEOL model of JSM-IT700HR, which was equipped with an energy-dispersive X-ray spectrometer (EDX). Another microscope (Keyence SEM VE-9800) was used for observation at low magnifications.

2.5.2. Mechanical Tests. A Shimadzu EZ-L testing machine was employed to measure the strength of circular or rectangular plates of RH at a fixed crosshead speed of 2 mm/min according to the Japan Industrial Standard (JIS A 5908).[36] Four to nine plate specimens were subjected to tests for each material to achieve a reliable average.

https://doi.org/10.1021/acsomega.2c03286
ACS Omega 2022, 7, 27638−27648

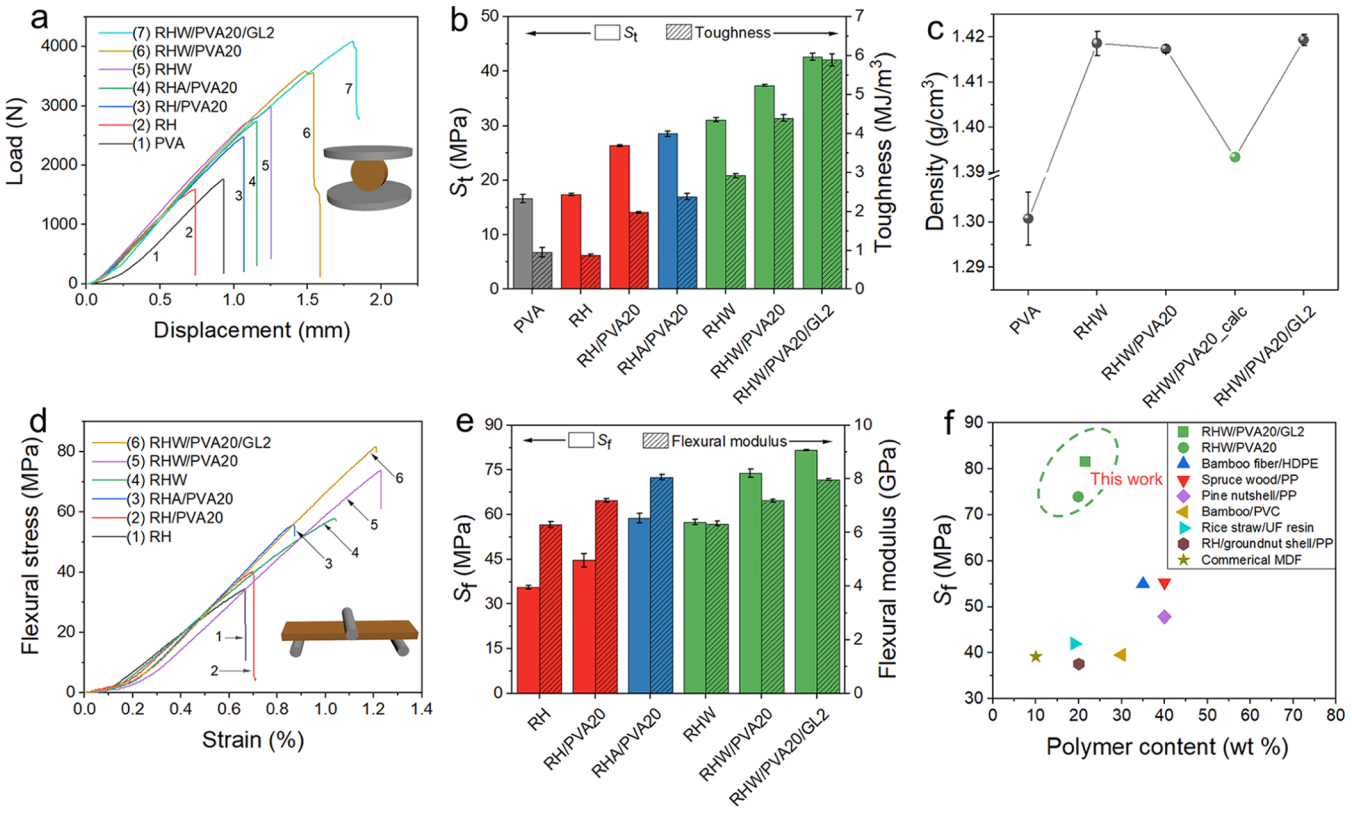

Figure 3. Mechanical properties of circular and rectangular plates. (a) Typical load−displacement curves for circular plates. (b) S_t and toughness of circular plates. (c) Apparent densities of circular plates. (d) Typical flexural stress−strain curves for rectangular plates. (e) S_f and flexural modulus of rectangular plates. (f) Comparison of S_f of RHW/PVA20 and RHW/PVA20/GL2 rectangular plates with that of reported materials.[3,19−21,47−49]

The overall tensile strength of circular plates was measured by applying a diametrical compressive force until the fracture of the specimen.[37,38] Tensile strength (S_t) was obtained by $S_t = 2F/(\pi dh)$,[37] where F is the maximum applied force, d is the diameter of the circular plate, and h is the thickness of the circular plate. Here, the toughness can be evaluated by dividing the fracture energy by the volume of the circular plate, while the fracture energy was calculated by integrating the stress with respect to strain.[39,40] Three-point bending tests with a fixed span of 32 mm were performed to determine the flexural strength (S_f) of the rectangular plate. $S_f = 3FL/(2bh^2)$,[41] where F is the maximum applied force, L is the length of the support span, b is the plate width, and h is the plate thickness. The flexural modulus was calculated from the slope of the linear portion of the stress−strain curves.[42]

2.5.3. Water Uptake and Swelling. The water uptake behavior of each material was investigated. The specimen (circular plate) was dried at 105 °C for 24 h in an oven. Its mass and thickness were measured. The plate was soaked in ultrapure water at 25 °C for 24 h or longer up to 624 h, according to JIS A 5908.[36] At the end of the soaking period, the plate was taken out of the water, and the mass and thickness were measured immediately upon the quick removal of surface water with tissue paper. Some materials were tested in repeated soaking−drying cycles. Each cycle consisted of soaking for 4 h at 25 °C and drying at 50 °C for 20 h as per the American National Standard (ANSI/HPVA HP-1, 2004).[43] The total carbon concentration (TOC) of the spent water was measured with a TOC analyzer (Shimadzu TOC-VCPH).

The water uptake and thickness swelling ratio were calculated by the following equations, respectively

$$\text{water uptake} = (m - m_0)/m_0$$

$$\text{thickness swelling ratio} = (d - d_0)/d_0$$

m_0 and m denote the mass of the plate before and after soaking, respectively. d_0 and d are the thicknesses of the plate, defined in the same way as for m_0 and m.

3. RESULTS AND DISCUSSION

3.1. Properties of RH and RHW. Figure 2a−f shows the optical and SEM photographs of RH and RHW before and after pulverization, together with their chemical compositions. The HCW treatment removed the hemicellulose, lignin, and ash (represented by silica) to degrees of removal of 66, 35, and 51%, respectively. This resulted in higher cellulose content in RHW than in RH. The surface of RH was covered by silica-rich bumps before pulverization. Such bumps seemed to be partially broken by the HCW treatment. This was caused by the removal of silica as well as hemicellulose and lignin. The pulverization of RHW caused the formation of not only particles with sizes smaller than 100 μm but also fibers with length (average; ca. 180 μm) and diameter (average; ca. 12 μm), as shown in Figures 2f and S1. Such fibrous particles hardly occurred during the pulverization of RH, while rod-shaped particles appeared. It was believed that the appearance of fibrous particles, in other words, macroscopic defibering, resulted in the removal of hemicellulose and lignin that had been associated with bundles of cellulose-rich fibers. The alkaline treatment seemed to have significantly damaged the fibers. As shown in Figure S2, fibrous particles were rarely found in the pulverized RHA, which consisted mainly of

https://doi.org/10.1021/acsomega.2c03286
ACS Omega 2022, 7, 27638−27648

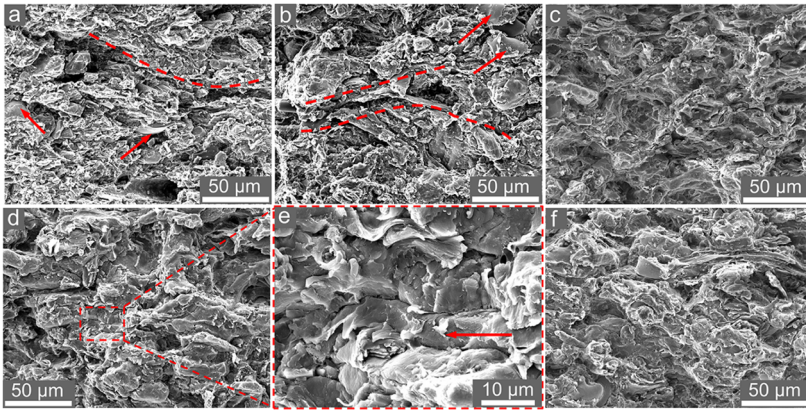

Figure 4. SEM images of fracture surfaces of circular plates: (a) RH, (b) RH/PVA20, (c) RHW, (d, e) RHW/PVA20, and (f) RHW/PVA20/GL2.

particles with sizes smaller than those of RH and RHW. Figure 2g–i shows the surface morphologies of RHW fibrous particles before and after blending with PVA or PVA/GL. Fiber surfaces were coated with PVA, although the coating was not necessarily complete.

3.2. Mechanical Strength. The mechanical properties of circular and rectangular plates of RH, RHW, and composites were investigated. Figure 3 summarizes the results. Figure 3a gives load–displacement relationships for circular plates. The loads increase linearly or semilinearly with the displacement until breakage and with similar slopes. The load at the breakage corresponds to the S_t, as shown in Figure 3b. The differences in the S_t among the materials were attributed mainly to those in the displacement upon breakage, i.e., the toughness.

It is clear that the plate strength was increased by the HCW treatment because the HCW treatment loosened the inherent recalcitrant structure of RH by removing the hemicellulose and lignin almost completely and partially, respectively, thereby inducing the occurrence of fibrous particles. The enrichment of cellulose-rich fibrous particles could interlock and fold under pressing and then enhance the strength by suppressing the development of cracks.[24] The remaining lignin acted as a binder and also promoted the strength during hot pressing. Afterward, the strength was further increased by blending with PVA as well as PVA/GL. It was strongly suggested that adhesion occurred between RHW and PVA via hydrogen bonds and between RHW and lignin, which had similar cohesive energies to PVA.[44,45] It was also believed that hydroxyl-rich PVA and GL acted as a binder and plasticizer in PVA–RHW composites, respectively. These roles will be discussed later.

The strength of the RH/PVA20 plate was greater than that of RH alone but much smaller than that of RHW/PVA20. This indicated that the HCW treatment had a positive effect on the incorporation of PVA into the RH matrix and/or adhesion between them. This was supported by SEM observation of the fracture surfaces of plates, as described later.

As shown in Figure 3c, the measured density of the RHW/PVA20 plate was clearly greater than the calculated value with a general assumption of volume additivity. This was consistent with not only the above-described good adhesion but also the implication of penetration of a portion of softened PVA into the RHW matrix. The effect of the PVA/RHW mass ratio on the S_t was explored, of which results are reported in Figure S3. Blending PVA at a mass fraction over 20 wt % caused a decrease in strength. This was because the inherent strength of the hot-pressed PVA was lower than that of RHW.

The S_t of the RHW/PVA20/GL2 plate, 42 MPa, was greater than those of RHW and RH plates by factors of 1.4 and 2.5, respectively. In addition, the toughness of the RHW/PVA20/GL2 plate, 5.9 MJ/m^3, was 6.7 times that of the RH plate. It was believed that GL acted as a plasticizer in PVA, or otherwise, PVA and RHW, enhancing adhesion between these two materials.[34,46] The effects of the GL content on S_t and toughness were investigated. The result is shown in Figure S4. Adding GL at a small fraction of up to 2–3 wt % to RHW/PVA20 significantly improved both S_t and toughness, but adding a greater fraction reduced them. The fraction of GL was thus optimized and fixed at 2 wt %. It was also found that the RHA/PVA20 plate had a smaller S_t than the RHW/PVA20 plate. This was probably because the alkaline treatment resulted in the excess removal of lignin and silica as matrix and reinforcing materials, respectively.

Flexural properties are significant because they are measures for determining plate deflections and buckling loads in exterior and interior applications.[10] As shown in Figure 3d,e, the trend of S_f followed that of S_t. The blending with PVA and PVA/GL enhanced the S_f of the RHW plate (57 MPa) by up to 74 and 81 MPa, respectively. The RHW/PVA20/GL2 plate also exhibited a superior strain upon breakage and flexural modulus to those of the RH plate. This demonstrated improvements in both toughness and stiffness. As seen in Figure 3f, the S_f of RHW/PVA20 and RHW/PVA20/GL2 composites also exceeds those of other types of composites such as medium-density fiberboard (MDF) with 34 MPa and some lignocellulose composites containing binders such as formaldehyde-based resins or blended with nonbiodegradable plastics.

3.3. Physical and Chemical Properties. Figure 4 displays SEM photographs of the fracture surfaces of circular plates. The surface of the RH plate had voids and gaps between layers, where stress concentration could occur in the lead-up to breakage (Figure 4a). Exposure of smooth surfaces (indicated by arrows in Figure 4b) is an indication of the poor bonding of inherent silica-rich bumps to the matrix. The occurrence of such voids, gaps, and bumps seemed to be suppressed by the HCW treatment, but the surface showed signs of bumps peeling from the matrix upon breakage, as shown in Figure 4c. The above-mentioned observations were hardly made for RHW/PVA20 (Figure 4d,e). Its fracture surface showed that PVA coated RHW particles homogeneously, as indicated by

https://doi.org/10.1021/acsomega.2c03286
ACS Omega 2022, 7, 27638–27648

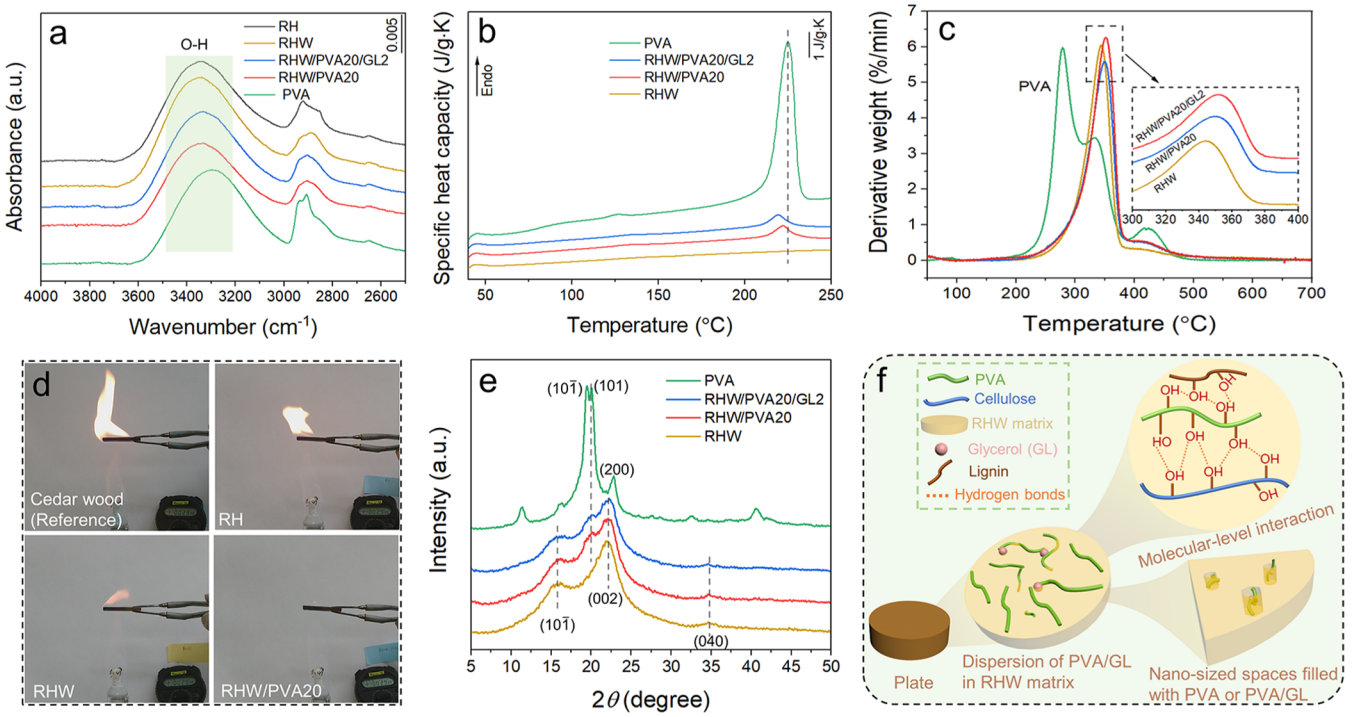

Figure 5. Physicochemical characterizations of hot-pressed PVA and prepared RHW-based composites. (a) FTIR spectra, (b) apparent specific heat capacity measured by DSC, (c) rates of mass release upon heating in TGA, (d) video screenshots of ignition/combustion tests of wood, RH, RHW, and RHW/PVA20 for 30 s (videos are in the Supporting Information), (e) XRD patterns, and (f) illustration of the interaction of PVA with RHW components.

the arrow, and then suppressed the local roughness of the surface. The difference between RH/PVA20 and RHW/PVA20 also demonstrated that the HCW treatment can significantly promote the adhesion of PVA to the RH matrix. The fracture surface of PHW/PVA20/GL2 was similar to that of RHW/PVA20 but had fewer cracks (Figure 4f). This was consistent with the effect of adding GL on the mechanical properties of RHW/PVA20. According to local images of the fracture surfaces of RHW and RHW/PVA20/GL2 (Figure S5), the former had some spaces (gaps) between nonbonded particles, while the latter had no such spaces. This was consistent with the magnitude relations of S_t and toughness for those two materials. SEM−energy-dispersive X-ray (SEM−EDX) analysis confirmed the dispersion of silica particles with sizes of up to 20 μm in the matrix (Figure S6), which positively affected the strength of the composite.[50] Fracture surfaces of RHA/PVA20 had more voids, cracks, and local roughnesses than RHW/PVA20. An SEM photograph is available in Figure S2. It was expected that the alkaline treatment greatly improved the adhesion between the matrix and PVA, but such an improvement was supported by neither mechanical properties nor fracture surfaces. The SEM−EDX analysis hardly detected silica on the fracture surface, which was expected from the removal of silica by alkaline treatment.

3.4. Physicochemical Characterizations of Hot-Pressed RH, RHW, PVA, and Their Composites. Figure 5 presents the physical, chemical, and thermochemical properties of the materials, which were evaluated by FTIR, DSC, TGA, combustion tests, and XRD. Figure 5a compares the FTIR spectra of different hot-pressed materials. The absorption band over the range of 3000−3600 cm^{-1}, assigned to the O−H stretching vibration, is influenced by the strength of hydrogen bonds between the −OH groups.[51] The absorption peaks for the hot-pressed PVA and RHW were centered at 3290−3300 and 3340−3350 cm^{-1}, respectively. The peak centers for RHW/PVA20 and RHW/PVA20/GL2 were very close to that for RHW. These characteristics suggested that the environment surrounding PVA was changed by the blending, in other words, at least a portion of PVA interacted with RHW via hydrogen bonds instead of strong hydrogen bonds within PVA.[52] For examining such an interaction, the hot-pressed PVA and hot-pressed RHW were pulverized and mixed manually at a mass ratio of 20:80 (referred to as the RHW/PVA20_mix), and the FTIR spectrum of the mixture was measured and compared with that of RHW/PVA20. As shown in Figure S7a, the absorption peak of the RHW/PVA20 composite shifted slightly to the higher wavenumber side (the region marked by a cycle showed a greater difference), and then the migration of PVA into the RHW matrix was confirmed.

Figure 5b compares the DCS profiles for the hot-pressed PVA, RHW, and their composites. The PVA underwent an endothermic peak centered at 225.0 °C, which was attributed to melting. Such an endothermic peak appeared upon heating of the composites but with smaller quantities of heat than expected with an assumption of additivity of the heat quantity. The peak temperatures for RHW/PVA20 and RHW/PVA20/GL2, 222.5 and 219.5 °C, respectively, were lower than that for PVA alone. This was explained by the fact that PVA was confined in nanosized small spaces in the matrix or, otherwise, dissolved into the matrix.[53,54] A mixture of the hot-pressed PVA and RHW (20:80 mass ratio), as a reference material, was analyzed under the same conditions as those for the composite (Figure S7b). It was then found that the quantities of heat (given as the peak area) arising from the melting of PVA were as small as 35 and 27% of that for the mixture, respectively, for

https://doi.org/10.1021/acsomega.2c03286
ACS Omega 2022, 7, 27638−27648

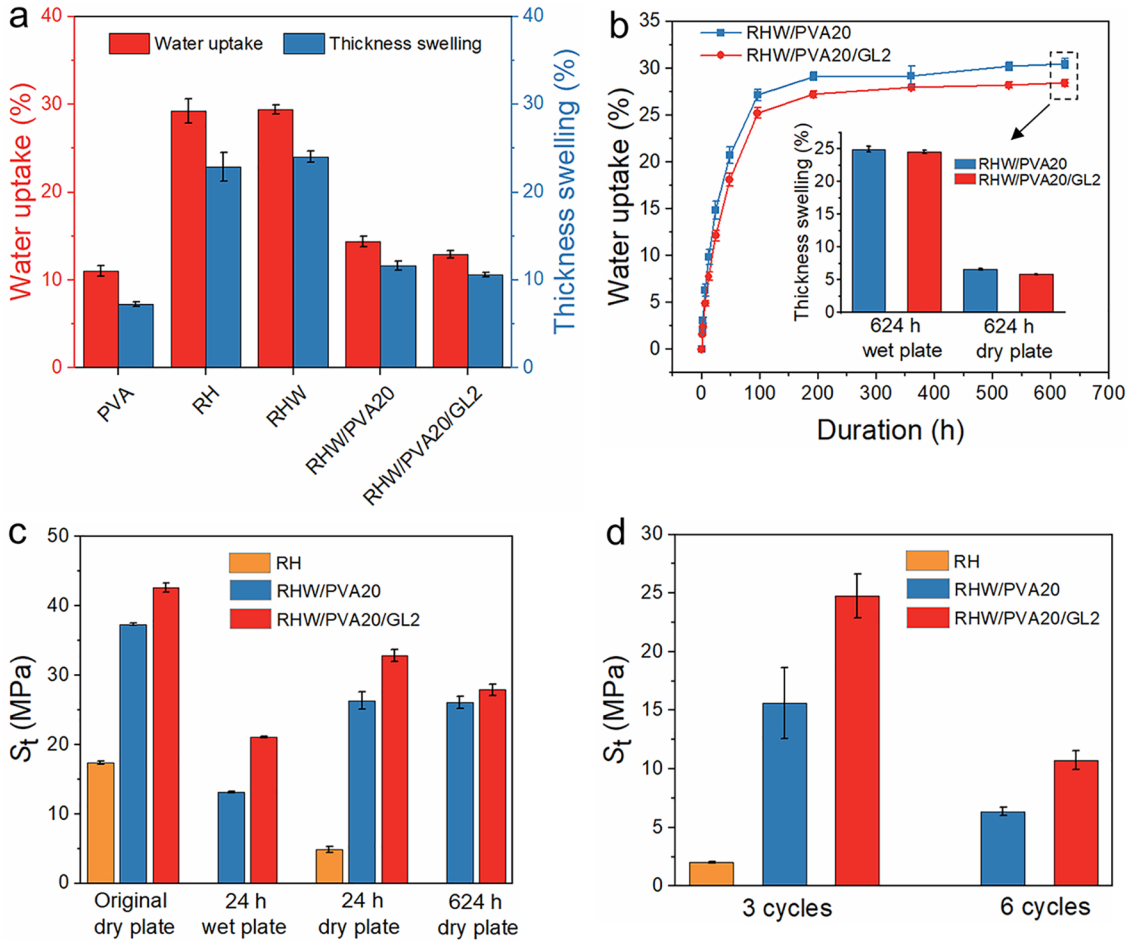

Figure 6. Measurement of waterproofness of different plate samples. (a) Water uptake and swelling ratio according to the thickness for soaking in 25 °C water for 24 h. (b) Time-dependent changes in water uptake for the long-term soaking of RHW/PVA20 and RHW/PVA20/GL2 plates at 25 °C (inset is the thickness swelling of wet plates at the end of soaking and sequentially dried plates at 50 °C). (c) S_t of RH, RHW/PVA20, and RHW/PVA20/GL2 plates at different states (wet plate represents the plate that has not been dried after soaking). (d) Impact of water soaking−drying cycle tests on S_t of plates of RH and composites.

RHW/PVA20 and RHW/PVA20/GL2. Such smaller quantities of heat were explained in the same way as above. It was difficult to conclude whether dissolution or nanodispersion occurred, but the PVA−RHW interaction via hydrogen bonds was unquestionable.

The thermal stability of the hot-pressed materials was investigated by TGA. The results are presented in Figure 5c. The profile of the mass release rate from PVA consisted of three peaks centered at 278, 333, and 420 °C. The first and second peaks are assigned to the decomposition of the −OH groups, while the third one is assigned to that of the main chains.[55] Both the first and second peaks were not detected for the composites. This evidenced copyrolysis of PVA and RHW, which occurred through their close contact or mixing at a molecular level. It was also found that the temperature for the maximum rate of mass release from RHW, T_{max}, of 344 °C shifted in the copresence of PVA and also PVA/GL to ca. 350 and 352 °C, respectively. These peaks arose mainly from the pyrolysis of cellulose.[56] In addition, T_{max} of the hot-pressed PVA/RHW, 348 °C, was lower than that of RHW/PVA20 (Figure S7c). Thus, the results indicated that the thermal stabilities of not only PVA but also RHW were improved by their interaction via hydrogen bonds, in particular, those between PVA and cellulose.

Figure 5d shows the results of combustion tests of RH, RHW, and RHW/PVA20 together with hot-pressed wood (a Japanese cedar) as a reference. RH seemed to have the advantage of suppressed flammability over the woody biomass, probably due to its lower organic matter content (i.e., higher silica content).[57] The flammability of RH was reduced by HCW treatment (i.e., to RHW conversion) due to the extensive removal of the hemicellulose and further reduced by blending with PVA or PVA/GL. The degrees of mass release from RH, RHW, RHW/PVA20, and RHW/PVA20/GL2 under an air atmosphere were compared (Figure S8). The mass release from RHW was smaller than that from RH at lower temperatures of 200−310 °C. The difference in the mass release (i.e., the degree of suppression of mass release) reached 10.6 wt %. The mass release from RHW/PVA20 was initially slightly greater than that from RHW at 200−295 °C because the composite contained 20 wt % of PVA, which was much more volatile than RHW. Nevertheless, the mass release from the composite up to 300−500 °C was smaller than that from RHW with a maximum difference of 13.2 wt %. This also demonstrated a greater suppressed flammability of RHW/PVA20. Considering the nearly colorless flame from the RHW/PVA20 composite in the combustion test, it was speculated that combustible matter was less abundant in the

https://doi.org/10.1021/acsomega.2c03286
ACS Omega 2022, 7, 27638−27648

volatiles from the composite and also that hydrogen bonds between RHW and PVA led to the formation of more water and cross-links from dehydration condensation of the −OH groups and, thereby, smaller amounts of oligomers and monomers from RHW and PVA. It was also noticed that the mass release profiles for RHW/PVA20 and RHW/PVA20/GL2 were very similar (Figure S8c), which was expected given the combustion characteristics of those two materials. The suppressed flammability of the composite was associated with a relevant feature, which was flame retardancy. This was consistent with the above-described higher thermal stabilities of RHW/PVA20 and RHW/PVA20/GL2 than both of their components.

Figure 5e compares XRD patterns of hot-pressed PVA, RHW, and their composites. Diffraction peaks at 16, 22, and 34.5° for RHW-based samples are assigned to $(10\bar{1})$, (002), and (040) planes of crystalline cellulose I, respectively.[58,59] Semicrystalline PVA shows diffraction peaks at 19.5−20° due to the $(10\bar{1})$ and (101) planes and another one at 23° assigned to the (200) plane.[60] The $(10\bar{1})$/(101) peak of PVA seemed to be suppressed in the composite, and this was an indication of the incorporation of a portion of PVA into the RHW matrix. Then, the diffractogram of RHW/PVA20 was compared with the 80:20 mixture of the hot-pressed/pulverized RHW and PVA. Its diffractogram is available together with that of RHW/PVA20 in Figure S7d. The suppression of PVA's $(10\bar{1})$ and (101) peaks was thus confirmed.

Figure 5a−e and some figures in the Supporting Information revealed the interaction between RHW and PVA via hydrogen bonds in their composite and also in RHW/PVA20/GL2, which is illustrated in Figure 5f. The above-described analytical results also showed that a portion of PVA was incorporated into the RHW matrix, and the incorporation was promoted by GL as a plasticizer. The interaction and adhesion between the PVA and the RHW matrix promoted the mechanical performance and thermal stability of their composite. It was believed that the other portion of PVA was dispersed in the RHW matrix having its own nanosized phases, which interacted with RHW at their interfaces.

3.5. Water Uptake and Swelling. From a perspective of fiberboard performance standards, it is desired to not only maximize the mechanical strength of plates but also minimize their water absorptivity. The water uptake and swelling ratio in the thickness direction of the plates were initially evaluated, as shown in Figure 6a. The results of soaking in water for 24 h revealed that the RHW plate had similar water uptake (∼30%) to the RH plate. When blended with PVA, RHW absorbed less water, 14.4%, which was roughly half of that without the blending. The thickness swelling also followed the same trend as the water uptake. The thickness swelling ratio of the RHW/PVA20/GL2 plate was as small as 11%, which was superior to the JIS A 5908 standard.[36] The swelling ratio was also smaller than that of the RH plate by a magnitude relationship of 53%. The dimensional stability of the plate was thus improved by the HCW treatment, blending with PVA, and the addition of GL. The water uptake by the RHW/PVA20/GL2, 12.9%, was even smaller than that without GL, despite its very high hydrophilicity. This suggests that GL is associated with PVA and RHW molecules via strong hydrogen bonds, which were not easily dissociated by water molecules.[61] Thus, GL not only acted as a plasticizer but also suppressed water uptake. These trends, taken together with the smallest water uptake and swelling ratio by the PVA plate, highlight the importance of bonding between PVA phases and RHW matrix via hydrogen bonds for suppressing the diffusion of water molecules into the RHW matrix. As shown in Figure 2h,i fibrous particles were coated with PVA before hot pressing. PVA after hot pressing in the composite could act as a diffusion barrier against water. It was also noted that the hot pressing of PVA at 200 °C caused dehydration condensation between the −OH groups, giving PVA cross-links and some hydrophobicity.[62] It was believed that more extensive densification, which left a smaller volume of interstitial spaces among primary particles in the plate, contributed to the slowdown of the water diffusion and penetration into the plate.

The spent water from the soaking was analyzed by TOC to measure the extraction of organic matter during the soaking. As shown in Figure S9a, the retention of organic carbon after 24 h of soaking was 99.98, 99.96, and 99.88% for RHW/PVA20, PVA, and RHW/PVA20/GL2, respectively. Slightly more extraction from RHW/PVA20/GL2 could be attributed to GL. Figure S9b demonstrates that the present RHW/PVA composites had smaller water uptake than some reported materials. This characteristic is important for water resistance.

Long-term stability was assessed for the plates of RH, RHW/PVA20, and RHW/PVA20/GL2, extending the soaking time by up to 624 h. As shown in Figure 6b, the water uptake by the composites increased to 28−30% and became steady at ca. 200−300 h. At 624 h, the swelling ratios were ca. 25%, which were roughly equivalent to those for RH and RHW after only 24 h. This was consistent with the role PVA played as a diffusion barrier against water, as speculated above. The composites, after 624 h of soaking, were dried in air at 50 °C for 20 h. The thickness of the dried plate was slightly greater than before the soaking. The cycle of swelling in water and the subsequent shrinkage (by drying) was irreversible. The degree of irreversible expansion was as small as 5−6%.

It was believed from the above-mentioned irreversible swelling−shrinkage cycle that the diffusion of water into the plate and the resulting swelling more or less physically deteriorated it. Then, the strengths of wet and dry plates were measured. As seen in Figure 6c, the strengths of wet composite plates were clearly lower than the original strengths but were recuperated to 71−78% by the subsequent drying. It was also confirmed that the recuperation of the composite strength was 61−65% after 624 h of soaking and drying. On the other hand, the strength of the RH plate decreased to only 28% of the original plate after 24 h of soaking and drying. It was thus demonstrated that the HCW treatment and subsequent blending with PVA were effective for not only the strength of hot-pressed plates but also water resistance. It was expected that the improvement of waterproofness, together with the near-complete hemicellulose removal and partial lignin removal, also improved mildew resistance.[57,63]

Plates of RH and the composites were subjected to more severe tests with three and six cycles of soaking and drying. Both composites experienced a loss in their strength. As shown in Figure 6d, their strengths after six cycles were 17−25% of their initial strengths. It thus seemed that the loss of strength continuously decreased with cycles. It was also found that the more water-resistant material, which was evaluated by the water uptake and swelling ratio after 24 h of soaking, experienced a lower rate of strength loss and a greater rate of recuperation.

Figure S10 displays the top and fracture surfaces of the composites before soaking, after a soaking−drying cycle, and

https://doi.org/10.1021/acsomega.2c03286
ACS Omega 2022, 7, 27638−27648

after three cycles. It seemed that repeated soaking−drying cycles caused and expanded cracks on the surface. The occurrence of cracks, which could act as stress concentration points, resulted in a reduction of S_t. Traces of structural deterioration were found on fracture surfaces. Those after one and three cycles had recesses, which occurred through the peeling of particles off the matrix upon breakage to form the surface. Physical structural deterioration was thus confirmed by the SEM observation of composite surfaces.

4. CONCLUSIONS

The HCW-treated RH, i.e., RHW, was pulverized and blended with PVA and fabricated into composite plates by the hot pressing molding. PVA acted as binder filling voids/gaps in the RHW matrix and adhered to it via hydrogen bonds. Moreover, a portion of PVA penetrated into the RHW matrix forming hydrogen bonds. The third component, GL, behaved as a plasticizer during hot pressing and then was retained in the PVA and/or the RHW matrix by hydrogen bonds. These roles of PVA and GL were revealed by the characterization of plates by density and analytical results from FTIR, DSC, TGA, and XRD. The combination of HCW treatment and blending with PVA and PVA/GL enhanced the mechanical performances of RHW plates, improving the S_t and S_f of RH plates from 17 to 42 and 36 to 81 MPa, respectively, while increasing the toughness 6.7 times. These superior mechanical performances were associated with superior water resistance, which was demonstrated by a smaller water uptake and thickness swelling ratio in water, a smaller loss of S_t after water soaking/drying cycles, and greater S_t recuperation during drying. Both PVA and GL thus contributed to the improved water resistance, despite their high hydrophilicities. Suppressed flammability was another feature of the combination of HCW treatment and blending with PVA. Hydrogen bonds between RHW and PVA suppressed the formation of combustible volatile matter at 200−400 °C. In summary, this study demonstrated how waste RH could be transformed into densified material with good properties in an environmentally friendly way, which will provide a sustainable approach for the utilization of agricultural wastes.

■ ASSOCIATED CONTENT

Supporting Information

The Supporting Information is available free of charge at https://pubs.acs.org/doi/10.1021/acsomega.2c03286.

Size distribution of fibrous parties involved in RHW after pulverization; SEM images of surface of RHA, pulverized RHA particles and fracture surface of the RHA/PVA20 plate; relationship between S_t /density and PVA contents in the composites; effect of the GL content on S_t and toughness of RHW−PVA−GL composites; SEM images of fracture surfaces of RHW and RHW/PVA20/GL2 at relatively high magnifications; SEM−EDX analysis of the fracture surface of RH, RHA/PVA20, RHW/PVA20, and RHW/PVA20/GL2; comparison of RHW/PVA20 and RHW/PVA20_mix in FTIR, DSC, TGA, and XRD tests; mass release profiles for RH, RHW, RHW/PVA20, and RHW/PVA20/GL2 under air atmosphere; TOC measurement and comparison of water uptake between RHW/PVA20, RHW/PVA20/GL2, and other similar densified materials; and SEM images of the top and fracture surfaces of plates after soaking/drying (PDF)

Combustion experiment of the wood plate—reference sample (Video S1) (MP4)

Combustion experiment of the original RH plate (Video S2) (MP4)

Combustion experiment of the RHW plate (Video S3) (MP4)

Combustion experiment of the RHW/PVA20 plate (Video S4) (MP4)

■ AUTHOR INFORMATION

Corresponding Author

Jun-ichiro Hayashi − *Interdisciplinary Graduate School of Engineering Sciences, Kyushu University, Kasuga, Fukuoka 816-8580, Japan; Institute for Materials Chemistry and Engineering and Research and Education Center of Green Technologies, Kyushu University, Kasuga, Fukuoka 816-8580, Japan;* orcid.org/0000-0001-5068-4015; Phone: +81 92 583 7796; Email: junichiro_hayashi@cm.kyushu-u.ac.jp; Fax: +81 92 583 7793

Authors

Qianli Wang − *Interdisciplinary Graduate School of Engineering Sciences, Kyushu University, Kasuga, Fukuoka 816-8580, Japan;* orcid.org/0000-0002-2033-0977

Shinji Kudo − *Interdisciplinary Graduate School of Engineering Sciences, Kyushu University, Kasuga, Fukuoka 816-8580, Japan; Institute for Materials Chemistry and Engineering and Research and Education Center of Green Technologies, Kyushu University, Kasuga, Fukuoka 816-8580, Japan;* orcid.org/0000-0003-0002-796X

Shusaku Asano − *Interdisciplinary Graduate School of Engineering Sciences, Kyushu University, Kasuga, Fukuoka 816-8580, Japan; Institute for Materials Chemistry and Engineering, Kyushu University, Kasuga, Fukuoka 816-8580, Japan;* orcid.org/0000-0001-6297-057X

Complete contact information is available at: https://pubs.acs.org/10.1021/acsomega.2c03286

Notes

The authors declare no competing financial interest.

■ ACKNOWLEDGMENTS

This study was financially supported by the Council for Science, Technology and Innovation (CSTI), the Cross-ministerial Strategic Innovation Promotion Program (SIP), "Technologies for Smart Bioindustry and Agriculture" administered by the Bio-oriented Technology Research Advancement Institution, and the National Agriculture and Food Research Organization (NARO). The authors are very grateful for the support of the Cooperative Research Program of Network Joint Research Center for Materials and Devices, which was funded by the Ministry of Education, Culture, Sports, Science, and Technology, Japan. Q.W. acknowledges Phatchada Santawaja for her assistance in some tests and is also grateful for the financial support provided by the China Scholarship Council Scholarship.

https://doi.org/10.1021/acsomega.2c03286
ACS Omega 2022, 7, 27638−27648

REFERENCES

(1) Gröndahl, J.; Karisalmi, K.; Vapaavuori, J. Micro- and nanocelluloses from non-wood waste sources; processes and use in industrial applications. *Soft Matter* **2021**, *17*, 9842−9858.
(2) Lim, J. S.; Manan, Z. A.; Alwi, S. R. W.; Hashim, H. A review on utilisation of biomass from rice industry as a source of renewable energy. *Renewable Sustainable Energy Rev.* **2012**, *16*, 3084−3094.
(3) El-Kassas, A. M.; Mourad, A. H. I. Novel fibers preparation technique for manufacturing of rice straw based fiberboards and their characterization. *Mater. Des.* **2013**, *50*, 757−765.
(4) Hýsková, P.; Hýsek, Š.; Schönfelder, O.; Šedivka, P.; Lexa, M.; Jarský, V. Utilization of agricultural rests: Straw-based composite panels made from enzymatic modified wheat and rapeseed straw. *Ind. Crops Prod.* **2020**, *144*, No. 112067.
(5) Gao, Y.; Xing, F. R.; Jha, M.; Yadav, K. K.; Yadav, R.; Matharu, A. S. Toward Novel Biocomposites from Unavoidable Food Supply Chain Wastes and Zirconia. *ACS Sustainable Chem. Eng.* **2020**, *8*, 14039−14046.
(6) He, X.; Wang, D. F.; Zhang, Y. L.; Tang, Y. Manufacturing Technology and Parameter Optimization for Composite Board from Corn Stalk Rinds. *BioResources* **2016**, *11*, 4564−4578.
(7) Wu, Z. Z.; Aladejana, J. T.; Liu, S. Q.; Gong, X. H.; Wang, X. A.; Xie, Y. Q. Unsaturated Polyester Resin as a Nonformaldehyde Adhesive Used in Bamboo Particle Boards. *ACS Omega* **2022**, *7*, 3483−3490.
(8) Kremensas, A.; Kairytė, A.; Vaitkus, S.; Vėjelis, S.; Członka, S.; Strąkowska, A. The impact of hot-water-treated fibre hemp shivs on the water resistance and thermal insulating performance of corn starch bonded biocomposite boards. *Ind. Crops Prod.* **2019**, *137*, 290−299.
(9) Muramatsu, H.; Kim, Y. A.; Yang, K. S.; Cruz-Silva, R.; Toda, I.; Yamada, T.; Terrones, M.; Endo, M.; Hayashi, T.; Saitoh, H. Rice Husk-Derived Graphene with Nano-Sized Domains and Clean Edges. *Small* **2014**, *10*, 2766−2770.
(10) Kwon, J. H.; Ayrilmis, N.; Han, T. H. Enhancement of flexural properties and dimensional stability of rice husk particleboard using wood strands in face layers. *Composites, Part B* **2013**, *44*, 728−732.
(11) Mohanty, A. K.; Vivekanandhan, S.; Pin, J. M.; Misra, M. Composites from renewable and sustainable resources: Challenges and innovations. *Science* **2018**, *362*, 536−542.
(12) Li, R. J.; Gutierrez, J.; Chung, Y. L.; Frank, C. W.; Billington, S. L.; Sattely, E. S. A lignin-epoxy resin derived from biomass as an alternative to formaldehyde-based wood adhesives. *Green Chem.* **2018**, *20*, 1459−1466.
(13) Hemmilä, V.; Adamopoulos, S.; Karlsson, O.; Kumar, A. Development of sustainable bio-adhesives for engineered wood panels - A Review. *RSC Adv.* **2017**, *7*, 38604−38630.
(14) Chalapud, M. C.; Herdt, M.; Nicolao, E. S.; Ruseckaite, R. A.; Ciannamea, E. M.; Stefani, P. M. Biobased particleboards based on rice husk and soy proteins: Effect of the impregnation with tung oil on the physical and mechanical behavior. *Constr. Build. Mater.* **2020**, *230*, No. 116996.
(15) Abbott, A. P.; Conde, J. P.; Davis, S. J.; Wise, W. R. Starch as a replacement for urea-formaldehyde in medium density fibreboard. *Green Chem.* **2012**, *14*, 3067−3070.
(16) Trinh, B. M.; Ogunsona, E. O.; Mekonnen, T. H. Thin-structured and compostable wood fiber-polymer biocomposites: Fabrication and performance evaluation. *Composites, Part A* **2021**, *140*, No. 106150.
(17) Chen, R. S.; Ahmad, S. Mechanical performance and flame retardancy of rice husk/organoclay-reinforced blend of recycled plastics. *Mater. Chem. Phys.* **2017**, *198*, 57−65.
(18) Suhot, M. A.; Hassan, M. Z.; Aziz, S. A.; Daud, M. Y. M. Recent Progress of Rice Husk Reinforced Polymer Composites: A Review. *Polymers* **2021**, *13*, No. 2391.
(19) Guna, V.; Ilangovan, M.; Rather, M. H.; Giridharan, B. V.; Prajwal, B.; Krishna, K. V.; Venkatesh, K.; Reddy, N. Groundnut shell / rice husk agro-waste reinforced polypropylene hybrid biocomposites. *J. Build. Eng.* **2020**, *27*, No. 100991.
(20) Wang, C. Q.; Mei, J.; Zhang, L. High-added-value biomass-derived composites by chemically coupling post-consumer plastics with agricultural and forestry wastes. *J. Cleaner Prod.* **2021**, *284*, No. 124768.
(21) Qian, S.; Wang, H.; Zarei, E.; Sheng, K. Effect of hydrothermal pretreatment on the properties of moso bamboo particles reinforced polyvinyl chloride composites. *Composites, Part B* **2015**, *82*, 23−29.
(22) Nasir, M.; Khali, D. P.; Jawaid, M.; Tahir, P. M.; Siakeng, R.; Asim, M.; Khan, T. A. Recent development in binderless fiber-board fabrication from agricultural residues: A review. *Constr. Build. Mater.* **2019**, *211*, 502−516.
(23) Xie, Q.; Li, F. Y.; Li, J. F.; Wang, L. M.; Li, Y. L.; Zhang, C. W.; Xu, J.; Chen, S. A new biodegradable sisal fiber-starch packing composite with nest structure. *Carbohydr. Polym.* **2018**, *189*, 56−64.
(24) Wang, Q.; Kudo, S.; Asano, S.; Hayashi, J.-i. Hot-Compressed Water Treatment and Subsequent Binderless Hot Pressing for High-Strength Plate Preparation from Rice Husk. *ACS Sustainable Chem. Eng.* **2022**, *10*, 1932−1942.
(25) Ding, L.; Li, X.; Hu, L. C.; Zhang, Y. C.; Jiang, Y.; Mao, Z. P.; Xu, H.; Wang, B. J.; Feng, X. L.; Sui, X. F. A naked-eye detection polyvinyl alcohol/cellulose-based pH sensor for intelligent packaging. *Carbohydr. Polym.* **2020**, *233*, No. 115859.
(26) Wang, H. M.; Yuan, T. Q.; Song, G. Y.; Sun, R. C. Advanced and versatile lignin-derived biodegradable composite film materials toward a sustainable world. *Green Chem.* **2021**, *23*, 3790−3817.
(27) Bian, H. Y.; Wei, L. Q.; Lin, C. X.; Ma, Q. L.; Dai, H. Q.; Zhu, J. Y. Lignin-Containing Cellulose Nanofibril-Reinforced Polyvinyl Alcohol Hydrogels. *ACS Sustainable Chem. Eng.* **2018**, *6*, 4821−4828.
(28) Hancock, B. C.; York, P.; Rowe, R. C. The use of solubility parameters in pharmaceutical dosage form design. *Int. J. Pharm.* **1997**, *148*, 1−21.
(29) Sameni, J.; Krigstin, S.; Sain, M. Solubility of lignin and acetylated lignin in organic solvents. *BioResources* **2017**, *12*, 1548−1565.
(30) Lamaming, J.; Heng, N. B.; Owodunni, A. A.; Lamaming, S. Z.; Abd Khadir, N. K.; Hashim, R.; Sulaiman, O.; Kassim, M. H. M.; Hussin, M. H.; Bustami, Y.; Amini, M. H. M.; Hiziroglu, S. Characterization of rubberwood particleboard made using carboxymethyl starch mixed with polyvinyl alcohol as adhesive. *Composites, Part B* **2020**, *183*, No. 107731.
(31) Wu, M. X.; Shuai, H.; Cheng, Q. F.; Jiang, L. Bioinspired Green Composite Lotus Fibers. *Angew. Chem., Int. Ed.* **2014**, *53*, 3358−3361.
(32) Zhang, X.; Liu, W. F.; Liu, W. Q.; Qiu, X. Q. High performance PVA/lignin nanocomposite films with excellent water vapor barrier and UV-shielding properties. *Int. J. Biol. Macromol.* **2020**, *142*, 551−558.
(33) Majeed, K.; Arjmandi, R.; Al-Maadeed, M. A.; Hassan, A.; Ali, Z.; Khan, A. U.; Khurram, M. S.; Inuwa, I. M.; Khanam, P. N. Structural Properties of Rice Husk and its Polymer Matrix Composites: An Overview. In *Lignocellulosic Fibre and Biomass-Based Composite Materials*; Elsevier, 2017; pp 473−490.
(34) Rahman, W. A. W. A.; Sin, L. T.; Rahmat, A. R.; Samad, A. A. Thermal behaviour and interactions of cassava starch filled with glycerol plasticized polyvinyl alcohol blends. *Carbohydr. Polym.* **2010**, *81*, 805−810.
(35) Sluiter, A.; Hames, B.; Ruiz, R.; Scarlata, C.; Sluiter, J.; Templeton, D.; Crocker, D. Determination of Structural Carbohydrates and Lignin in Biomass. In *Laboratory Analytical Procedure*; National Renewable Energy Laboratory: Golden, CO, 2012.
(36) Japanese Industrial Standard*JIS A 5908−2003 Particleboards*; Japanese Standards Association: Tokyo, Japan, 2003.
(37) Mori, A.; Yuniati, M. D.; Mursito, A. T.; Kudo, S.; Norinaga, K.; Nonaka, M.; Hirajima, T.; Kim, H. S.; Hayashi, J.-i. Preparation of Coke from Indonesian Lignites by a Sequence of Hydrothermal Treatment, Hot Briquetting, and Carbonization. *Energy Fuels* **2013**, *27*, 6607−6616.
(38) Namburi, D. K.; Singh, K.; Huang, K. Y.; Neelakantan, S.; Durrell, J. H.; Cardwell, D. A. Improved mechanical properties

https://doi.org/10.1021/acsomega.2c03286
ACS Omega 2022, 7, 27638−27648

through recycling of Y-Ba-Cu-O bulk superconductors. *J. Eur. Ceram. Soc.* **2021**, *41*, 3480−3492.
(39) Hakalahti, M.; Salminen, A.; Seppälä, J.; Tammelin, T.; Hänninen, T. Effect of interfibrillar PVA bridging on water stability and mechanical properties of TEMPO/$NaClO_2$ oxidized cellulosic nanofibril films. *Carbohydr. Polym.* **2015**, *126*, 78−82.
(40) Amiri, H.; Kianmehr, M. H.; Arabhosseini, A. Effect of particle size, die rotary speed and amount of urea on physical properties of the produced pellet. *Int. J. Environ. Sci. Technol.* **2019**, *16*, 2059−2068.
(41) Mahmood, H.; Moniruzzaman, M.; Yusup, S.; Akil, H. M. Pretreatment of oil palm biomass with ionic liquids: a new approach for fabrication of green composite board. *J. Cleaner Prod.* **2016**, *126*, 677−685.
(42) Sitz, E. D.; Bajwa, D. S. The mechanical properties of soybean straw and wheat straw blended medium density fiberboards made with methylene diphenyl diisocyanate binder. *Ind. Crops Prod.* **2015**, *75*, 200−205.
(43) Pang, H. W.; Wang, Y. Y.; Chang, Z. W.; Xia, C. L.; Han, C. R.; Liu, H. G.; Li, J. Z.; Zhang, S. F.; Cai, L. P.; Huang, Z. H. Soy meal adhesive with high strength and water resistance via carboxymethylated wood fiber-induced crosslinking. *Cellulose* **2021**, *28*, 3569−3584.
(44) Haque, A. N. M. A.; Zhang, Y.; Naebe, M. A review on lignocellulose/poly (vinyl alcohol) composites: cleaner approaches for greener materials. *Cellulose* **2021**, *28*, 10741−10764.
(45) Ago, M.; Okajima, K.; Jakes, J. E.; Park, S.; Rojas, O. J. Lignin-Based Electrospun Nanofibers Reinforced with Cellulose Nanocrystals. *Biomacromolecules* **2012**, *13*, 918−926.
(46) Wang, W. T.; Zhang, H.; Jia, R.; Dai, Y. Y.; Dong, H. Z.; Hou, H. X.; Guo, Q. B. High performance extrusion blown starch/polyvinyl alcohol/clay nanocomposite films. *Food Hydrocolloids* **2018**, *79*, 534−543.
(47) Mu, B. S.; Tang, W.; Liu, T.; Hao, X. L.; Wang, Q. W.; Ou, R. X. Comparative study of high-density polyethylene-based biocomposites reinforced with various agricultural residue fibers. *Ind. Crops Prod.* **2021**, *172*, No. 114053.
(48) Krause, K. C.; Müller, M.; Militz, H.; Krause, A. Enhanced water resistance of extruded wood-polypropylene composites based on alternative wood sources. *Eur. J. Wood Wood Prod.* **2017**, *75*, 125−134.
(49) Shams, M. I.; Yano, H. Development of selectively densified surface laminated wood based composites. *Eur. J. Wood Wood Prod.* **2009**, *67*, 169−172.
(50) Song, H. Z.; Zheng, L. W. Nanocomposite films based on cellulose reinforced with nano-SiO_2: microstructure, hydrophilicity, thermal stability, and mechanical properties. *Cellulose* **2013**, *20*, 1737−1746.
(51) Hu, J. Q.; Wu, Y. L.; Yang, Q.; Zhou, Q. W.; Hui, L. F.; Liu, Z.; Xu, F.; Ding, D. Y. One-pot freezing-thawing preparation of cellulose nanofibrils reinforced polyvinyl alcohol based ionic hydrogel strain sensor for human motion monitoring. *Carbohydr. Polym.* **2022**, *275*, No. 118697.
(52) Xu, X. D.; Li, L. J.; Seraji, S. M.; Liu, L.; Jiang, Z.; Xu, Z. G.; Li, X.; Zhao, S.; Wang, H.; Song, P. A. Bioinspired, Strong, and Tough Nanostructured Poly(vinyl alcohol)/Inositol Composites: How Hydrogen-Bond Cross-Linking Works. *Macromolecules* **2021**, *54*, 9510−9521.
(53) Singh, M. P.; Singh, R. K.; Chandra, S. Properties of Ionic Liquid Confined in Porous Silica Matrix. *Chemphyschem* **2010**, *11*, 2036−2043.
(54) Shalom, T. B.; Nevo, Y.; Leibler, D.; Shtein, Z.; Azerraf, C.; Lapidot, S.; Shoseyov, O. Cellulose nanocrystals (CNCs) induced crystallization of polyvinyl alcohol (PVA) super performing nanocomposite films. *Macromol. Biosci.* **2019**, *19*, No. 1800347.
(55) Aloui, H.; Khwaldia, K.; Hamdi, M.; Fortunati, E.; Kenny, J. M.; Buonocore, G. G.; Lavorgna, M. Synergistic Effect of Halloysite and Cellulose Nanocrystals on the Functional Properties of PVA Based Nanocomposites. *ACS Sustainable Chem. Eng.* **2016**, *4*, 794−800.
(56) Deng, J.; Xiong, T. Y.; Wang, H. Y.; Zheng, A. M.; Wang, Y. Effects of Cellulose, Hemicellulose, and Lignin on the Structure and Morphology of Porous Carbons. *ACS Sustainable Chem. Eng.* **2016**, *4*, 3750−3756.
(57) Chen, Y. P.; Dang, B. K.; Fu, J. Z.; Wang, C.; Li, C. C.; Sun, Q. F.; Li, H. Q. Cellulose-Based Hybrid Structural Material for Radiative Cooling. *Nano Lett.* **2021**, *21*, 397−404.
(58) Segal, L.; Creely, J. J.; Martin, A. E., Jr.; Conrad, C. M. An empirical method for estimating the degree of crystallinity of native cellulose using the X-ray diffractometer. *Text. Res. J.* **1959**, *29*, 786−794.
(59) Buendia-Kandia, F.; Mauviel, G.; Guedon, E.; Rondags, E.; Petitjean, D.; Dufour, A. Decomposition of Cellulose in Hot-Compressed Water: Detailed Analysis of the Products and Effect of Operating Conditions. *Energy Fuels* **2018**, *32*, 4127−4138.
(60) Liu, P.; Chen, W. H.; Liu, C. H.; Tian, M.; Liu, P. J. A novel poly (vinyl alcohol)/poly (ethylene glycol) scaffold for tissue engineering with a unique bimodal open-celled structure fabricated using supercritical fluid foaming. *Sci. Rep.* **2019**, *9*, No. 9534.
(61) Kusmono; Wildan, M. W.; Lubis, F. I. Fabrication and Characterization of Chitosan/Cellulose Nanocrystal/Glycerol Bio-Composite Films. *Polymers* **2021**, *13*, No. 1096.
(62) Xie, Y. J.; Pan, Y. F.; Cai, P. X. Hydroxyl crosslinking reinforced bagasse cellulose/polyvinyl alcohol composite films as biodegradable packaging. *Ind. Crops Prod.* **2022**, *176*, No. 114381.
(63) Hosseinaei, O.; Wang, S.; Rials, T. G.; Xing, C.; Taylor, A. M.; Kelley, S. S. Effect of Hemicellulose Extraction on Physical and Mechanical Properties and Mold Susceptibility of Flakeboard. *For. Prod. J.* **2011**, *61*, 31−37.

https://doi.org/10.1021/acsomega.2c03286
ACS Omega 2022, 7, 27638−27648